



# Comparative Analysis of the Efficiency of Scalar and Vector-Scalar Antennas for Onboard Receiving Systems

Artem Kharakhashyan<sup>(✉)</sup>

Department of Applied Mathematics, Don State Technical University, Rostov-on-Don, Russia  
artemharashyan@mail.ru

**Abstract.** The signal detection and the determination of its location are the recurrent problems in a large number of scientific and industrial applications. Its effective solution requires the robust and precise signal processing methods as well as the advanced understanding of the possible sources of errors, one of which in the most cases is the background noise. This paper studies the characteristics of the target signal detection and source location estimation accuracy for an onboard hydroacoustic receiving system operating in presence of the background structural noise. All the methods considered are based on the conventional Bartlett's estimator but they are used to process the different components of the acoustic field, namely pressure, vibrational velocity and acoustic power flux. The high efficiency of the acoustic power flux method is demonstrated using numerical results and spatial spectra comparison.

**Keywords:** Acoustic power flux · Covariance · Structural noise · Vector-scalar · Vibrational velocity · Beamformer

## 1 Introduction

Nowadays, in order to achieve greater efficiency of hydroacoustic receiving systems that ensure the detection of low-noise objects and provide for stable underwater communication, an approach based on an increasingly complete extraction of information contained in the acoustic field is being intensively studied [1–5]. This is usually accomplished by using vector-scalar antennas that can measure acoustical pressure and vibrational velocity of the particles of the medium simultaneously. The most common of them are stationary, towed and onboard. The noise component that makes the largest contribution to the resulting noise field differs for each type of the antennas. For stationary systems, the greatest noise source corresponds to the noise of the sea surface and the water column, for towed ones, it relates to the flow-induced turbulent noise, and for onboard systems, it relates to the structural interference, which is produced by vibrations of the frame and hull elements of the carrier structure.

The main performance characteristics of onboard systems depend on the parameters of the structural noise. The most significant of them are the energy and statistical characteristics, which have not been studied deeply enough for a vector-scalar components

of structural noise. This is especially true for acoustic power flux components, which have been studied insufficiently.

The purpose of this paper is the analysis of the detection characteristics of a target signal and the accuracy of determining the location of its source during the operation of the onboard receiving system in the presence of a background structural noise. The research is carried out using computer modeling and experimental data processing for a set of detection methods: *P*-method, based on pressure measurements processing; *PV*-method, employing both pressure and particle velocity; and *W*-method, using acoustic power flux components.

Experimental characteristics of the structural noise are presented for the scalar and vector components of the acoustic field, as well as for the power flux. Based on the results of the calculations, a comparison of the performance characteristics of scalar and vector-scalar antennas is carried out according to the following metrics: the signal-to-noise ratio at the output of the receiving system, the probability of correct detection and false alarms, and the accuracy of the target azimuth assessment, namely the root-mean-square error and the mean absolute error.

## 2 Signal-Noise Model

The signals measured by the receiving system can be described via time-dependent functions of voltage at the inputs of the receiving elements. In the narrow-band approximation, the acoustic field at the input of the antenna array is characterized by an *M*-dimensional vector *U*, whose elements are equal to:

$$U_m(\omega_n) = \frac{1}{\sqrt{T}} \int_{-T/2}^{T/2} u_m(t) e^{-j\omega_n t} dt, \omega_n = \frac{2\pi n}{T}, m = 1 \dots 4M, \tag{1}$$

where *t* is the time,  $\omega_n$  is the angular frequency. The elements of the vector *U* are the coefficients of the Fourier series expansion of  $u_m(t)$  calculated from the signal measurement samples of duration *T*. The data vector obtained after performing the Fourier transform is:

$$U^* = (P \ V_x \ V_y \ V_z), \tag{2}$$

where *P*, *V<sub>x</sub>*, *V<sub>y</sub>*, *V<sub>z</sub>* are the vectors with size *M*. For sound pressure  $P^* = (P_1, P_2, \dots, P_M)$ , and for vector components (projections of vibrational velocity on the coordinate axes, expressed in equivalent units of sound pressure of the plane acoustic wave)  $V_x^* = (V_{x1}, V_{x2}, \dots, V_{xM})$ ,  $V_y^* = (V_{y1}, V_{y2}, \dots, V_{yM})$  and  $V_z^* = (V_{z1}, V_{z2}, \dots, V_{zM})$ ; the symbol “\*” means Hermitian conjugate.

The direction to the target signal is described via a pair of spatial angles in the spherical coordinate system, that is the azimuth  $\theta_0$  and the elevation  $\varphi_0$  [6]. The spectral response at the pressure receiver of the *m*-th sensor, obtained as a result of the Fourier transform of the input signal, equals to  $P_{Sm} = A_S[\exp(-jkx_m \cos\theta_0 \sin\varphi_0)]$ , where  $m = 1, \dots, M$ ,  $\lambda$  is the wavelength corresponding to the center frequency *f* of the narrowband filter,  $k = 2\pi/\lambda$  is a wavenumber,  $x_m = d[m - (M + 1)/2]$  is the coordinate of the *m*-th

sensor,  $d$  is the distance between sensors,  $A_S$  is the signal amplitude at the receiver's point.

Using the direction cosines as weights for the vibrational velocity components, the vector  $\mathbf{U}$  for a signals received from an infinitely remote target can be represented as  $\mathbf{U}_S = (1, \cos\theta_0 \sin\varphi_0, \sin\theta_0 \sin\varphi_0, \cos\varphi_0)^T \otimes \mathbf{P}$ , here “ $\otimes$ ” is the Kronecker product. The signals from an infinitely remote source are assumed to be a plane wave.

In hydroacoustics, signals propagating from radiation sources during non-turbulent excitation can be described as stationary random Gaussian processes with zero mean. In that case, the measurement statistics is completely determined by the covariance matrix, which is calculated as the product of a column vector and a complex conjugate row vector  $\mathbf{K} = \mathbf{U} \cdot \mathbf{U}^*$ .

The covariance matrix  $\mathbf{K}$  for a vector-scalar receiving antenna, consisting of  $M$  vector-scalar modules, will have a block form and a size of  $4M \times 4M$ :

$$\mathbf{K}_{PV} = \begin{pmatrix} \mathbf{P} \cdot \mathbf{P}^* & \mathbf{P} \cdot \mathbf{V}_x^* & \mathbf{P} \cdot \mathbf{V}_y^* & \mathbf{P} \cdot \mathbf{V}_z^* \\ \mathbf{V}_x \cdot \mathbf{P}^* & \mathbf{V}_x \cdot \mathbf{V}_x^* & \mathbf{V}_x \cdot \mathbf{V}_y^* & \mathbf{V}_x \cdot \mathbf{V}_z^* \\ \mathbf{V}_y \cdot \mathbf{P}^* & \mathbf{V}_y \cdot \mathbf{V}_x^* & \mathbf{V}_y \cdot \mathbf{V}_y^* & \mathbf{V}_y \cdot \mathbf{V}_z^* \\ \mathbf{V}_z \cdot \mathbf{P}^* & \mathbf{V}_z \cdot \mathbf{V}_x^* & \mathbf{V}_z \cdot \mathbf{V}_y^* & \mathbf{V}_z \cdot \mathbf{V}_z^* \end{pmatrix}. \quad (3)$$

Each of the four diagonal blocks of this  $M \times M$  sized matrix describes the covariance dependences between the same components of the vector-scalar acoustic field, and the off-diagonal blocks describe covariance between different components.

### 3 Signal Detection Methods

In this paper, the characteristics of a scalar and vector-scalar receiving system are analyzed for various beamforming approaches. Three signal processing methods have been used.

The first method performs an evaluation based on pressure measurements only, the covariance matrix estimate is formed as follows:

$$\hat{\mathbf{K}}_P = \mathbf{P} \cdot \mathbf{P}^*. \quad (4)$$

Hereinafter the subscript  $P$  means processing using only the scalar component of the acoustic field.

To compare the efficiency of the scalar and vector-scalar antennas the second method, employing both acoustical pressure and vibrational velocity, is considered. The covariance matrix has the form (3), the method will be denoted with the subscript  $PV$ .

The third method is based on processing the acoustic power flux  $W = \mathbf{P} \cdot \mathbf{V}^*$ , the covariance matrix (3) is transformed in such a way that it contains only acoustic power flux elements  $\mathbf{P} \cdot \mathbf{V}_r^*$  ( $r = x, y, z$ ):

$$\hat{\mathbf{K}}_W = \mathbf{P} \cdot \mathbf{V}_x^* \oplus \mathbf{P} \cdot \mathbf{V}_y^* \oplus \mathbf{P} \cdot \mathbf{V}_z^*. \quad (5)$$

The subscript  $W$  will be used to denote the acoustic power flux method, symbol “ $\oplus$ ” corresponds to the direct sum of square matrices:  $\mathbf{P} \cdot \mathbf{V}_x^*$ ,  $\mathbf{P} \cdot \mathbf{V}_y^*$  and  $\mathbf{P} \cdot \mathbf{V}_z^*$ .

All the signal processing methods under consideration are based on the Bartlett's beamformer:

$$Z(\theta) = \mathbf{B}^*(\theta) \cdot \hat{\mathbf{K}} \cdot \mathbf{B}(\theta), \quad (6)$$

The Bartlett's method performs linear transformations on the input signals, which do not change their statistical characteristics, what is essential for the  $W$ -method as acoustic power flux might have a non-normal distribution [7], making estimation process more complicated. Bartlett's beamformer method has a standard resolution, its output signal is proportional to the power of the received signals, which simplifies the physical interpretation of the results.

For the  $P$ -method with the covariance matrix (4), the steering vector in expression (6) is equal to:

$$\mathbf{B}_P(\theta) = \begin{pmatrix} \exp(jkx_1 \cos\theta) \\ \exp(jkx_2 \cos\theta) \\ \vdots \\ \exp(jkx_M \cos\theta) \end{pmatrix}. \quad (7)$$

When using the approach involving all vector-scalar components of the acoustic field ( $PV$ -method) described by (3), the steering vectors are given in the form:

$$\mathbf{B}_{PV}(\theta) = (1, \cos\theta \sin\varphi, \sin\theta \sin\varphi, \cos\varphi)^T \otimes \mathbf{B}_P(\theta). \quad (8)$$

For the acoustic power flux of  $W$ -method (5), the spatial spectrum is calculated in accordance with the following expression:

$$Z_W(\theta) = \mathbf{B}_P^*(\theta) \cdot \hat{\mathbf{P}} \cdot \hat{\mathbf{V}}_x^* \cdot \mathbf{B}_x(\theta) \oplus \mathbf{B}_P^*(\theta) \cdot \hat{\mathbf{P}} \cdot \hat{\mathbf{V}}_y^* \cdot \mathbf{B}_y(\theta) \oplus \mathbf{B}_P^*(\theta) \cdot \hat{\mathbf{P}} \cdot \hat{\mathbf{V}}_z^* \cdot \mathbf{B}_z(\theta). \quad (9)$$

## 4 Experimental Setup

The experimental setup (Fig. 1) consisted of a steel plate with size  $2.55 \times 2.87 \text{ m}^2$  similar to the element of the vessel hull, the linear receiving antenna, 4 vibration generators and rod transducers were horizontally installed on the opposing sides of the plate. The receiving antenna was constructed from the two linear layers of sensors and was mounted on a noise-absorbing cover. Each layer included 6 acoustical pressure sensors. The distance between the centers of sensors was equal to 0.16 m (along  $X$ -axis). The distance between the two layers was 0.053 m (along  $Y$ -axis).

This design allows calculation of pressure gradient for frequencies, where the inter-element distance  $d \ll \lambda$  to obtain vibrational velocity. The scheme of the setup in the horizontal plane is shown in Fig. 2.

The experiment was conducted during calm weather on Ladoga Lake, Russia. The hull plate was submerged in water at the depth of 10 m, waveguide depth was 20 m. Speed of sound in water was 1430 m/s.

The legitimacy of measuring the vibrational velocity by calculating the pressure gradients from a pair of neighboring receivers for this design was verified experimentally. The vector receivers were calibrated during the experiment.



**Fig. 1** Experimental setup: view from the antenna side on the left, and view from the vibration generators side on the right

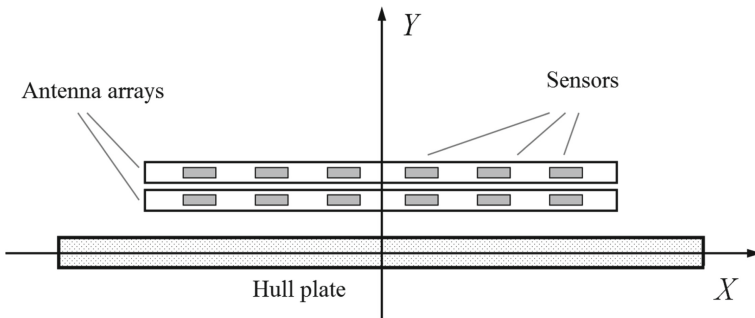


**Fig. 2** Diagram of the receiving antenna in a horizontal plane

## 5 Results and Discussion

The study of characteristics of the structural noise was carried out using computer simulation and via processing of experimental data. The detection characteristics of a target signal and the accuracy of determining the direction of arrival (DOA) of the target's signal were considered in presence of the structural noise.

### 5.1 Structural Noise Characteristics

The excitation of vibrations causing structural noise was carried out by means of four powerful vibration generators located on the side opposite to the receiving antenna. The vibration generators were set to asynchronous impulse mode such a way as to obtain a broadband random noise signal. The frequency domain spectrum of the noise on the pressure sensors is presented in Fig. 3.

Table 1 shows the covariance matrix structure with each cell element representing a component of the acoustic field.

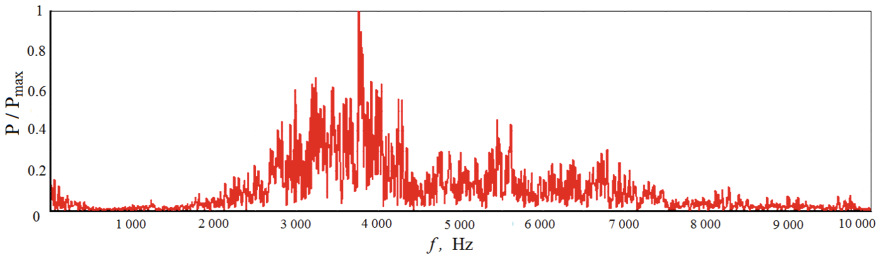


**Fig. 3** Noise spectrum during asynchronous excitation of the hull plate by vibrators

**Table 1** Covariance matrix structure

$K_{ij}$			
$P \cdot P^*$	$P \cdot V_x^*$	$P \cdot V_y^*$	$P \cdot V_z^*$
$V_x \cdot P^*$	$V_x \cdot V_x^*$	$V_x \cdot V_y^*$	$V_x \cdot V_z^*$
$V_y \cdot P^*$	$V_y \cdot V_x^*$	$V_y \cdot V_y^*$	$V_y \cdot V_z^*$
$V_z \cdot P^*$	$V_z \cdot V_x^*$	$V_z \cdot V_y^*$	$V_z \cdot V_z^*$

The real part of the normalized covariance matrix values calculated for the single sensor module located above the center of the plate for both the theoretical model presented in [8] and the empirical random sources model [9] are given in Table 2. Experimentally obtained results have been used to optimize the models and to achieve the coincidence of the simulation results with the experiment. Cells are organized according to Table 1 and values are normalized to the squared acoustical pressure value  $P \cdot P^*$ .

**Table 2** Real part of the normalized covariance matrix

Theoretical model				Random sources model			
1.00	0.00	-0.45	0.00	1.00	0.00	-0.45	-0.02
0.00	0.41	0.00	0.00	0.00	0.41	0.00	0.01
-0.45	0.00	0.26	0.00	-0.45	0.00	0.26	0.01
0.00	0.00	0.00	0.32	-0.02	0.01	0.01	0.33

An analysis of the results showed that the structural noise sound intensity for the acoustic power flux components is significantly lower than that of the scalar and vector components for both the models considered. The same applies for the experimental results.

One of the key indicators affecting the performance of receiving systems is the variance or standard deviation of the noise. The dependence of the structural noise variance

for the scalar and acoustic power flux components for the averaging time samples  $N_t$  is illustrated in Fig. 4. Data is provided in logarithmic scale.

The variance values for the acoustic power flux components are lower than those for the scalar component even at short averaging times and decrease faster depending on the averaging time. This factor is significant in further research and development of the detection algorithms, since the variance of the noise is inversely proportional to the efficiency of the receiving system according to many criteria, for example, the signal-to-noise ratio at the output of the receiving system and the probabilities of correct detection and false alarm.

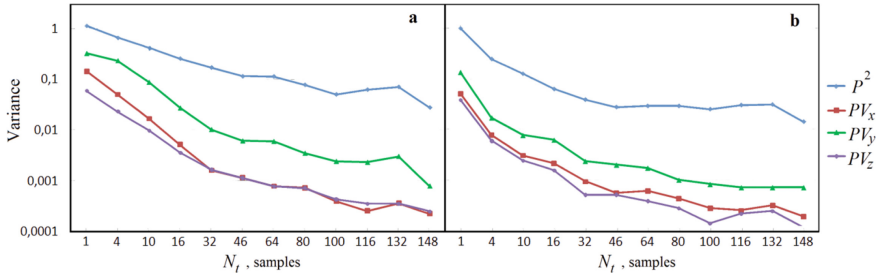


**Fig. 4** Noise variance for the scalar and acoustic power flux components: on the left (a) the experimental data; on the right (b) the simulation results

The coincidence of the experimental parameters of structural noise and the parameters obtained using computer simulation made it possible to calculate the main performance characteristics for scalar and vector-scalar antennas and to compare their efficiency for a set of signal-noise situations. The random sources model was chosen over the theoretical model due to its flexibility and simplicity.

### 5.2 Signal Detection and DOA Estimation Performance

The spatial spectra calculated using each corresponding method under the total effect of structural noise and a signal from an infinitely remote signal source are presented in Fig. 5. The calculations were performed using the respective processing methods.

The distance between the receiving antenna and the hull plate was 0.1 m, the plate has a size of  $3 \times 3 \text{ m}^2$ . Signal-to-noise ratio at the input was set to 1/40. The calculation was conducted at 3000 Hz. Spatial spectra are normalized to the maximum value of the output spectrum for each corresponding method separately. For example, for the  $P$ -method the normalization is performed by the value of  $Z_{max} = \max(Z(\theta))$ .

Based on the results, it was found out that the  $W$ -method produces a smaller main lobe width than the  $P$ - and  $PV$ -methods. The excess of the main lobe level over the noise level is also significantly higher for the  $W$ -method. For the considered signal-to-noise ratio, the  $W$ -method successfully detects the target at all target angles. According to the averaged spatial spectra for both  $P$ - and  $PV$ -methods, it was not always possible to detect the target signal against the background of noise, especially when the signal source is close to fore-and-aft directions.

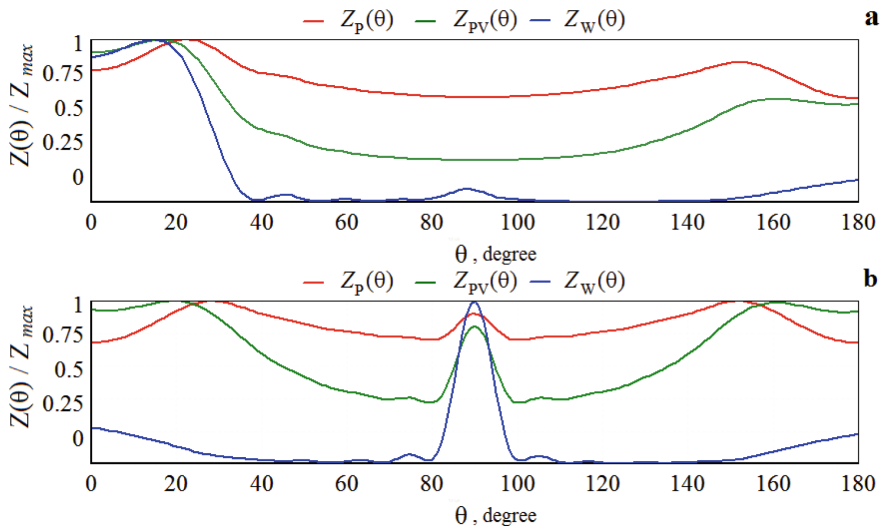


**Fig. 5** Spatial spectra corresponding to the total effect of the structural noise and the target signal; real target azimuth: (a)  $\theta_0 = 15^\circ$ , (b)  $\theta_0 = 90^\circ$

It is important to note that for a linear antenna, the spatial spectra obtained using the  $P$ - and  $PV$ -methods are characterized by the presence of two side lobes caused by structural noise. The  $W$ -method produces a relatively uniform spatial spectrum without distinct side lobes at fore-and-aft directions. This leads to a small number of systematic errors, thus providing a wider field of view of the antenna. Negative values for acoustic power flux method allow one to differentiate between the board side and sea side, improving the detection performance even more.

Signal detection characteristics such as signal-to-noise ratio at the output ( $\text{SNR}_{\text{out}}$ ) and correct detection probability are presented in Table 3. Detection probability was calculated using Neyman–Pearson test. The probability of false alarms was fixed at 0.01.

According to the results,  $W$ -method that employs acoustic power flux provides the highest signal-to-noise ratio at the output and the detection probability among the methods evaluated. Acoustical pressure-based method performs the worst, practically not detecting the target signal. Both  $\text{SNR}_{\text{out}}$  and detection probability decrease closer to fore-and-aft directions for all methods.

Signal direction of arrival estimation performance is shown in Table 4. The criteria considered are mean absolute error (MAE) and root-mean-square error (RMSE).

The accuracy of target azimuth estimation greatly decreases for angle ranges corresponding to the side lobes. As the  $W$ -method produces no distinct side lobes its performance decreases the least, MAE and RMSE estimates were less than  $1^\circ$  in most tests. For  $P$ -method DOA estimates are inconclusive, providing errors greater than  $5^\circ$ .  $PV$ -method achieved higher accuracy than  $P$ -method but still underperforms compared to  $W$ -method.



**Table 3** Signal detection performance

$\theta_0$ , degrees	SNR <sub>out</sub>			Detection probability		
	<i>P</i>	<i>PV</i>	<i>W</i>	<i>P</i>	<i>PV</i>	<i>W</i>
15	1.26	2.30	3.58	0.091	0.276	0.901
30	1.00	3.11	4.74	0.039	0.578	0.990
45	1.83	10.26	14.48	0.198	0.999	0.999
60	1.69	15.77	19.63	0.150	0.999	0.999
90	1.80	22.60	29.10	0.156	0.999	0.999

**Table 4** DOA estimation performance

$\theta_0$ , degrees	MAE, degrees			RMSE, degrees		
	<i>P</i>	<i>PV</i>	<i>W</i>	<i>P</i>	<i>PV</i>	<i>W</i>
15	5.92	1.12	0.09	6.28	1.34	0.94
30	1.00	2.17	0.09	1.95	2.53	1.01
45	4.72	2.61	0.03	7.88	5.09	0.36
60	5.35	1.81	0.01	10.81	5.84	0.11
90	0.09	0.01	0.02	6.60	0.20	0.13

## 6 Conclusions

Theoretical and experimental comparison of the characteristics of the structural noise showed that the variance for acoustic power flux components is lower and decrease faster than the variance for the scalar and vector components. As a result, when information is accumulated over a short time, the main characteristic of the receiving system (such as signal-to-noise ratio at the output), which processes the acoustic power flux measurements, can significantly exceed those of the scalar or conventional vector-scalar receiving systems.

It is shown that the best detection characteristics for all the considered criteria are obtained for the method that employs a vector-scalar antenna and uses acoustic power flux components in the data processing. The worst performance for all the considered criteria is observed for the method that uses only the scalar component of the acoustic field and is limited to acoustical pressure measurement. It is also important to note that when the direction of arrival of a signal from the target is close to the fore-and-aft aspects of the carrier, the *P*-method in most of the considered situations was not able to detect the signal at all, while the *W*-method has provided for target signal detection with a high probability.

Thus, it can be concluded that vector-scalar antennas, which allow for processing of acoustic power flux components, are promising and can be used to develop onboard

receiving systems that achieve greater target detection probability and DOA estimation accuracy.

## References

1. Kasatkin BA, Zlobina NV, Kasatkin SB, Kosarev GV (2022) IOP Conf Ser: Earth Environ Sci 988:032065
2. Zhang X et al (2021) Micromachines 12(2):168
3. Chen H, Zhu Z, Yang D (2022) J Mar Sci Eng 10:138
4. Dao F, Zeng Y, Zou Y, Li X, Qian J (2021) Energies 14:7840
5. Zhao A, Ma L, Hui J, Zeng C, Bi X (2018) J SensS 2018:1
6. Gordienko VA (2007) Vector-phase methods in acoustics. Fizmatlit, Moscow, p 480
7. Vorob'ev SD, Sizov VI (1992) Akusticheskij Zhurnal 38(4):654
8. Maslov VL, Budrin SV (2010) Control methods for acoustic signatures in engineering structures. Krylov State Research Centre, Saint Petersburg, p 328
9. Seleznev IA, Glebova GM, Zhbakov GA, Kharakhash'yan AM (2017) Underw Investig Robot 24(2):52